著者(英)	[illegible]
[illegible]	[illegible]
[illegible]	[illegible]
[illegible]	[illegible]
[illegible]	[illegible]
[illegible]	[illegible]
[illegible]	[illegible]

doi: 10.1109/TPEL.2017.2780088

IEEE TRANSACTIONS ON POWER ELECTRONICS

Title : A Single-Stage LED Driver based on ZCDS Class-E Current-Driven Rectifier as a PFC for Street-Lighting Applications

Author :

1. Satit Mangkalajan, *Student Member*, *IEEE*
2. Chainarin Ekkaravarodome*, *Member, IEEE*,
3. Kamon Jirasereeamornkul
4. Phatiphat Thounthong, *Senior Member*, *IEEE*
5. Kohji Higuchi
6. Marian K. Kazimierczuk, *Fellow, IEEE*

Address :

1. Department of Electronic and Telecommunication Engineering, Faculty of Engineering, King Mongkut's University of Technology Thonburi, Bangkok 10140, Thailand
2. Department of Instrumentation and Electronics Engineering, Faculty of Engineering, King Mongkut's University of Technology North Bangkok, Bangkok 10800, Thailand
3. Department of Electronic and Telecommunication Engineering, Faculty of Engineering, King Mongkut's University of Technology Thonburi, Bangkok 10140, Thailand
4. Department of Teacher Training in Electrical Engineering, Faculty of Technical Education, King Mongkut's University of Technology North Bangkok, Bangkok 10800, Thailand
5. UEC ASEAN Research Center, The University of Electro-Communications, Tokyo 182-8585, Japan
6. Department of Electrical Engineering, College of Engineering and Computer Science, Wright State University, Dayton, OH 45435, United States of America

E-mail :

1. satit_inse2009@hotmail.com
2. chainarin.e@eng.kmutnb.ac.th*
3. kamon.jir@mail.kmutt.ac.th
4. phatipat.t@fte.kmutnb.ac.th
5. higuchi@ee.uec.ac.jp
6. marian.kazimierczuk@wright.edu

A Single-Stage LED Driver based on ZCDS Class-E Current-Driven Rectifier as a PFC for Street-Lighting Applications

Satit Mangkalajan, *Student Member*, *IEEE*, Chainarin Ekkaravarodome*, *Member, IEEE*,
Kamon Jirasereeamornkul, Phatiphat Thounthong, *Senior Member*, *IEEE*,
Kohji Higuchi and Marian K. Kazimierczuk, *Fellow, IEEE*

Abstract—This paper presents a light-emitting diode (LED) driver for street-lighting applications that uses a resonant rectifier as a power-factor corrector (PFC). The PFC semi-stage is based on a zero-current and zero-derivative-switching (ZCDS) Class-E current-driven rectifier, and the LED driver semi-stage is based on a zero-voltage-switching (ZVS) Class-D *LLC* resonant converter that is integrated into a single-stage topology. To increase the conduction angle of the bridge-rectifier diodes current and to decrease the current harmonics that are injected in the utility line, the ZCDS Class-E rectifier is placed between the bridge-rectifier and a DC-link capacitor. The ZCDS Class-E rectifier is driven by a high-frequency current source, which is obtained from a square-wave output voltage of the ZVS Class-D *LLC* resonant converter using a matching network. Additionally, the proposed converter has a soft-switching characteristic that reduces switching losses and switching noise. A prototype for a 150-W LED street light has been developed and tested to evaluate the performance of the proposed approach. The proposed LED driver had a high efficiency (>91%), a high PF (>0.99), and a low THD_i (<8%) under variation of the utility-line input voltage from 180~250 V_{rms}. These experimental results demonstrate the feasibility of the proposed LED scheme.

Index Terms—Street-lighting system, LED driver, power-factor correction, soft-switching techniques, Class-E current-driven rectifier.

Footnote

Manuscript received……………………………..…; revised……………………………; accepted………………………… Date of publication………………………; date of current version……………………….. This work was supported in part by the National Research Council of Thailand and the King Mongkut's University of Technology North Bangkok under Grant No. KMUTNB-GOV-59-01, and in part by the Thailand Research Fund, the Commission on Higher Education, and King Mongkut's University of Technology North Bangkok under Grant No. TRG5880088. Recommended for publication by………………………
(Corresponding author: Chainarin Ekkaravarodome.)

Satit Mangkalajan and Kamon Jirasereeamornkul are with the Department of Electronic and Telecommunication Engineering, Faculty of Engineering, King Mongkut's University of Technology Thonburi, Bangkok 10140, Thailand (e-mail: satit_inse2009@hotmail.com; kamon.jir@mail.kmutt.ac.th).

Chainarin Ekkaravarodome is with the Advanced Power Electronics and Experiment Laboratory (APEx Lab), Department of Instrumentation and Electronics Engineering, Faculty of Engineering, King Mongkut's University of Technology North Bangkok, Bangkok 10800, Thailand (e-mail: chainarin.e@eng.kmutnb.ac.th).

Phatiphat Thounthong is with the Renewable Energy Research Centre (RERC), Department of Teacher Training in Electrical Engineering, Faculty of Technical Education, King Mongkut's University of Technology North Bangkok, Bangkok 10800, Thailand (e-mail: phatipat.t@fte.kmutnb.ac.th).

Kohji Higuchi is with the UEC ASEAN Research Center, The University of Electro-Communications, Tokyo 182-8585, Japan (e-mail: higuchi@ee.uec.ac.jp).

Marian K. Kazimierczuk is with the Department of Electrical Engineering, College of Engineering and Computer Science, Wright State University, Dayton, OH 45435, United States of America (e-mail: marian.kazimierczuk@wright.edu).

Digital Object Identifier ………………………………………………..………

I. Introduction

The conventional light sources for street-lighting systems that are using gas discharge lamps, such as high-pressure sodium vapor lamps and metal halide lamps, will inevitably be replaced by high-brightness light-emitting diodes (HB-LEDs) for the next generation of lighting applications. This replacement is due to the attractive characteristics of the latter source, including its high efficacy, good color-rendering index, long lifespan, ecological friendliness, and low price. HB-LEDs do not require high-striking voltage during starting and hot restarting. Table I shows some comparisons of the high-pressure sodium vapor lamps, metal halide lamps, and HB-LEDs for street-lighting systems. Typically, the rated lamp power of a commercialized LED street light lies between 60 W to 240 W [1]. An LED also requires a driving circuit called an LED driver to operate, which is similar to the ballast for the gas-discharge lamps. The main function of the LED driver is to convert a high-voltage alternating current (AC) from the utility line into a low-voltage direct current (DC) with constant-current control.

The generic implementation of a two-stage LED driver and a single-stage LED driver are presented in Fig. 1(a) and (b), respectively. Commonly, LED drivers for HB-LED employ two-stage topologies, which consist of a PFC stage and a DC-DC converter stage with constant-current control, as presented by many researchers [2]–[10]. These topologies are relatively easy to design because each part is separated. However, many power switches and control circuits in each stage are required, which leads to high costs and large size. Therefore, the two-stage topologies are suitable for high-power applications. To overcome these problems, single-stage topologies in which a PFC semi-stage and a DC-DC converter semi-stage are integrated into one as has been proposed by many researchers in recent years [11]–[39]. All the existing single-stage topologies can be classified based on the number of their power switches: usually a single switch or two switches. The main advantage of single-stage single-switch topologies [11]–[21] is a low cost. Additionally, these topologies are usually chosen for low-power applications, such as residential and commercial applications, due to the high-voltage stress. Single-stage two-switch topologies are usually suitable for medium-power applications. Nevertheless, the single-stage two-switch topologies [22]–[39] are chosen when system efficiency, the total harmonic distortion of the utility-line input current and a low DC-link voltage stress are the main design targets.

Some single-stage two-switch topologies have been proposed and based on resonant rectifiers, such as a PFC semi-stage [34]–[39]. The high-power-factor and the low-line current harmonic are achieved using the output characteristics of the resonant rectifier, which is placed between the front-end bridge-rectifier and a DC-voltage link. The various kinds of resonant rectifiers that are used as a power-factor corrector can be divided into two categories, as illustrated in Fig. 2. The first group is the zero-voltage-switching (ZVS) topologies, which can be further divided into two sub-groups: the Class-E- based topology, such as a Class-E current-driven rectifier that is used as a power-factor corrector (CECS-RPFC) [34]; and the Class-DE-based topology, such as a Class-DE current-driven rectifier that is used as a power-factor corrector (CDECS-RPFC) [35]–[37]. These ZVS rectifiers are operated under zero-voltage and zero-derivative switching (ZVDS) conditions. Despite their low-line current harmonic contents and high power-factor, the ZVS groups have a main problem of high-conduction losses in the power switches near the zero-crossing of the utility-line input voltage; this conduction loss leads to relatively low-system efficiency. The second group is the zero-current-switching (ZCS) topologies, which can be further divided into two sub-groups: the Class-D-based topology, such as a Class-D current-driven rectifier that is used as a power-factor corrector (CDCS-RPFC) [38], [39], which has a high system efficiency and a high total harmonic distortion (THD) of the utility-line input current; and the Class-E-based topology, which is the scheme proposed in this paper.

This paper presents a new topology of the RPFC family in which a ZCDS Class-E current-driven rectifier is used as a power-factor corrector (CECS-RPFC) of a single-stage LED street-light driver. The system efficiency, switching noise, and utility-line input current harmonic can be improved when compared with the previously reported ZVS-RPFC and ZCS-RPFC topologies. The step-by-step design procedures, power loss analysis, experimental validation of theory, and performance comparison are given.

II. Structure of Proposed LED Driver

A. Resonant Rectifier for Power-Factor Correction Concept

Fig. 3 depicts a conceptual diagram with key waveforms of the resonant rectifier as a power-factor corrector based on a ZCDS Class-E current-driven rectifier. The ZCDS Class-E current-driven rectifier is placed between the bridge-rectifier, and the DC-link capacitor is driven by a high-frequency current source. Additionally, a part of the ZCDS Class-E current-driven rectifier performs the function of a pass device across which the voltage difference v_O that is dropped. To increase the current conduction angle of the bridge-rectifier diodes and to decrease the current harmonics injected in the utility-line input, the DC-link voltage V_B should be higher than the peak of the rectified utility-line input voltage $|v_{in}|$, and the output voltage of the ZCDS Class-E current-driven rectifier v_O should be high near the zero crossing of the utility-line input voltage and low near the peak of the utility-line input voltage. The analysis and design of the proposed single-stage LED driver that is based on a ZCDS-CECS-RPFC is carried out under the following assumptions to simplify the analysis:

1) the power MOSFETs and the power diodes form an ideal switch whose on-state voltage equals zero, off-state is modeled by an infinite resistance, and switching time equals zero. However, their parasitic capacitor and anti-parallel diode of the power MOSFETs are considered as a function of the ZVS operation.
2) the passive components are linear and do not have parasitic components except for a transformer at the load matching network, which uses the transformer parasitic elements as resonant components.
3) the DC-filter capacitors are large enough that their voltages are approximately constant over one switching cycle and the *LC* input filter is not present in the circuit.
4) in the steady state, the LED is considered as a load resistor with a fixed resistance.

B. Circuit Description

The circuit diagram of the proposed single-stage LED driver of an LED street light with an output voltage and current controller is shown in Fig. 4. The presented single-stage LED driver consists of a bridge-rectifier D_1-D_2-D_3-D_4, a differential-mode electromagnetic interference (EMI) filter L_f-C_f, which is inserted on the DC side and serves as a filter to prevent the high-frequency current of the PFC semi-stage entering the bridge rectifier. Hence, the bridge-rectifier can use standard-recovery diodes. The ZCDS Class-E current-driven rectifier for the PFC contains a fast-recovery diode D_E and a high-frequency transformer T_1 as an isolating device and a part of the matching network. A series-resonant circuit L_{dc}-C_d

serves the function of high-frequency current shaping, which is fed by a square-wave output voltage υ_p from the ZVS Class-D *LLC* resonant converter and is converted into a high-frequency current source i_{dp} to drive the ZCDS Class-E current-driven rectifier. A DC-link capacitor C_B is charged by the PFC semi-stage and can be regarded as a voltage source that supplies the LED driver semi-stage [40]–[45]. The ZVS Class-D *LLC* resonant converter consists of a matching network C_r-L_r-L_{mD}, which must present an inductive load to ensure ZVS operation; a center-tapped transformer T_2 with a turns ratio of N_p:N_{s1}:N_{s2} = n_{LLC}:1:1, full-wave center-tapped rectifier D_{D1}-D_{D2}, and an output capacitor C_O. The transformer T_2 is also an isolation device and a part of matching network, where L_{mD} is the magnetizing inductance, and L_r is the transformer leakage inductance. A pair of bidirectional switches M_1-M_2 is operated with a duty ratio of approximately 0.5. Each switch is comprised of a transistor and an anti-parallel diode. The metal-oxide-semiconductor field-effect transistors (MOSFETs) are preferred devices because their body diodes can be used for operation above resonance. A dual control loop of a constant voltage (CV) and a constant current (CC) controller, part number SEA05 (STMicroelectronics), is used to detect the output voltage through the resistive voltage divider and the output current through the current sensing resistor. The output signal of the CV/CC controller is fed into a variable-frequency controller with gate driver part number L6599 (STMicroelectronics) via the photocoupler, part number PC851 (Sharp Microelectronics).

C. Operating Principle

The operation principle of the ZCDS Class-E current-driven rectifier in the PFC semi-stage is described by an equivalent circuit presented in Fig. 5(a). The two standard-recovery diodes D_1 and D_4 of the bridge-rectifier conduct during the positive half-cycle of the utility-line input voltage $\upsilon_{in} = V_{in} \sin \omega_L t$, where ω_L is a line angular frequency. The two standard-recovery diodes D_2 and D_3 conduct during the negative utility-line input half-cycle. The model of the positive utility-line input voltage rectifier output is a full-wave rectified sinusoidal voltage source $|\upsilon_{in}| = V_{in}|\sin\omega_L t|$. For simplicity sake, the fundamental-component approximation is used in the analysis of the rectifier with adequate accuracy. An inductance L_{mE} is a reflected magnetizing inductance from the primary side to the secondary side of the transformer T_1. To simplify the design procedure, assume that the transformer T_1 is ideal. Therefore, the transformer turns ratio is $n_{PFC} = N_p/N_s = \sqrt{L_p/L_s}$, where N_p and N_s are the winding numbers of the turns of the primary L_p and the secondary L_s inductors, respectively. If the inductance L_{mE} is large enough, then the current is approximately constant over one switching cycle and is equal to I_O, as depicted in Fig. 5(b). A high-frequency voltage source υ_p and a series inductor L_{dp} on the primary side of the transformer T_1 are reflected to the secondary side as a voltage source υ_s and an inductor L_{ds}, as illustrated in Fig. 5(c).

The high-frequency voltage source v_s and a series inductor L_{ds} is converted into a high-frequency current source i_{ds} to drive the ZCDS Class-E current-driven rectifier, as shown Fig. 5(d). The current waveform of the matching network that drives the ZCDS Class-E current-driven rectifier is assumed to be a sine-wave $i_{ds} = I_{ds}\sin(\omega_S t+\phi)$, where ω_S is the switching angular frequency. In this circuit, the DC-link voltage source V_B and the full-wave rectified sinusoidal voltage source $|v_{in}|$ are connected in series. Hence, these voltage sources can be combined into one voltage source $v_O = V_B - |v_{in}|$, as shown in Fig. 5(e). The output voltage of the ZCDS Class-E current-driven rectifier is forced by the voltage source $v_O = V_B - |v_{in}|$. This voltage leads to a varying load resistance R_L of the ZCDS Class-E current-driven rectifier. The equivalent circuit of the ZCDS Class-E current-driven rectifier for the PFC during the negative utility-line input half-cycle is similar to the equivalent circuit during the positive utility-line input half-cycle. Accordingly, the explanations are omitted. The important characteristic of the proposed ZCDS-CECS-RPFC is that the duty ratio D_e of the diode D_E in the ZCDS Class-E current-driven rectifier depends on the load resistance R_L. If the load resistance R_L of the ZCDS-CECS-RPFC is increased, while its high-frequency driving current is kept relatively constant, the output voltage v_O of the ZCDS-CECS-RPFC increases, and the diode duty ratio D_e is reduced. In other words, if the output voltage v_O of the ZCDS-CECS-RPFC is forced to a higher voltage than the nominal value, the diode duty ratio D_e of the ZCDS Class-E current-driven rectifier is automatically reduced. The average diode current automatically decreases as the output voltage v_O increases. Therefore, the output characteristics of the ZCDS Class-E current-driven rectifier with a varying load resistance roughly matches the output characteristics to achieve the proper operation of the power-factor correction, as presented in Fig. 3.

The operating modes in one switching cycle of the equivalent circuit of the ZCDS-CECS-RPFC during the positive and negative utility-line input half-cycles are given in Table II. When the diode D_E is turned on, the diode forward current i_E equals the difference of the high-frequency current source i_{ds} and the inductor current i_{LE}. The derivative of the diode forward current is zero at turn-on, and its absolute value reaches zero at turn-off. When the diode D_E is turned off, the diode reverse voltage v_E equals the difference of the output voltage v_O and the inductor voltage v_{LE}. The diode reverse voltage v_E has a step change at turn-off and a low absolute value of the derivative at turn-on. Therefore, the diode current i_E and diode voltage v_E of diode D_E are operated under the ZCS and ZCDS conditions $i_E(0) = 0$ and $di_E(\omega_S t)/d(\omega_S t)|_{\omega st=0} = 0$. In this case, switching losses and the switching noise level are reduced. The formulas further explaining these conditions can be found in reference [46].

Fig. 6 shows conceptual waveforms of the proposed single-stage LED driver. Figs. 6(a) and (b) show the sinusoidal utility-line input voltage v_{in} and the rectified utility-line input voltage $|v_{in}|$ waveforms. The combined voltage $V_B - |v_{in}|$ waveform is depicted in Fig. 6(c). If an instantaneous value of the utility-line input voltage v_{in} is positive and low near a zero crossing, the output voltage of the CECS-RPFC $v_O = V_B - |v_{in}|$ is high, and the diode duty ratio D_e of the ZCDS-CECS-RPFC diode current i_E is low. Consequently, the average value of the rectifier diode current $|i_{in}|$ over one switching cycle is low. Similarly, if an instantaneous value of the utility-line input voltage v_{in} is positive and high near a peak, the output voltage of the CECS-RPFC $v_O = V_B - |v_{in}|$ is low, and the diode duty ratio D_e of the ZCDS-CECS-RPFC diode current i_E is high. Accordingly, the average value of the rectifier diode current $|i_{in}|$ over one switching cycle is high. The amplitude of the high-frequency current source i_{dp} depends on the output voltage v_O of the ZCDS-CECS-RPFC. Thus, the waveform of the high-frequency current source i_{dp}, which is shown in Fig. 6(d), is high near the peak of the utility-line input voltage and low near the zero crossing of the utility-line input voltage in order to achieve a high-power-factor and low utility-line input current harmonics. Fig. 6(e) depicts the current i_s waveform of square-wave output voltage source at midpoint of the ZVS Class-D *LLC* resonant converter. Fig. 6(f) presents the rectifier diode current i_E of the ZCDS-CECS-RPFC. A conduction angle modulation of the bridge-rectifier diode current waveform without the EMI filter over the line frequency f_L and the line current i_{in} waveform are shown in Fig. 6(g). The negative utility-line input half-cycle is similar to the conceptual waveforms during the positive utility-line input half-cycle; hence, the descriptions are not presented.

If the switching frequency f_S is much higher than the line frequency f_L, then the high-frequency current source i_{ds} is approximately constant for one switching cycle and equals the output current i_O of the ZCDS-CECS-RPFC. The key current and voltage waveforms in one switching cycle of the proposed single-stage LED driver are shown in Fig. 7. A detailed analysis of the complete operation of the ZVS Class-D *LLC* resonant converter, including the six stages, can be found in references [40]–[45].

D. Circuit Analysis

The principle of operation of the proposed single-stage LED driver is explained by the equivalent circuit that is shown in Fig. 8(a). The input impedance of the ZCDS Class-E current-driven rectifier is represented by a series combination of an input resistor R_{ip} and the input inductor L_{ip}, which is reflected from the secondary side of the transformer T_1. Additionally, the matching network C_r-L_r-L_{mD}, the center-tapped transformer T_2 with turns ratio of n_{LLC}:1:1, the full-wave center-tapped rectifier diodes D_{D1}-D_{D2}, the output filter capacitor C_O, and the street-lighting LEDs are transformed into the AC-equivalent circuit C_r-L_r-L_{mD}-R_p, as presented in Fig. 8(b). The series inductor circuit L_{ip}-L_{dp} is replaced by an equivalent inductor $L_{idp} = L_{ip}+L_{dp}$. The MOSFETs are modeled by switches with on-resistances r_{DS1} and r_{DS2}. The resistance r_{Ldt} represents the equivalent winding resistances of the inductors L_{dp} with the transformer T_1 and the resistance r_{Lrt} represents the equivalent winding resistance of the transformer T_2. Therefore, the equivalent circuits of the ZVS Class-D *LLC* resonant converter are modeled by a square-wave voltage source υ_{DS2} with an equivalent resistor $r_S = (r_{DS1}+r_{DS2})/2 \approx r_{DS}$ and are loaded by two series circuits r_{Ldt}-C_d-L_{idp}-R_{ip} and r_{Lrt}-C_r-L_{rm}-R_s as depicted in Fig. 8(c).

An equivalent circuit of the PFC semi-stage with an equivalent sine-wave voltage source is presented in Fig. 9(a). The high-frequency voltage source at midpoint of the ZVS Class-D *LLC* resonant converter through a matching network are reflected from the primary side to the secondary side of the transformer T_1, as depicted in Fig. 9(b). The model of the proposed LED street-light driver can be divided into two parts: a simplified circuit of the ZCDS-CECS-RPFC and an equivalent circuit of the ZVS Class-D *LLC* resonant converter semi-stage, as depicted in Figs. 9(c) and (d), respectively. From Fig. 9(b), the minimum value of the load resistance $R_{L\min}$ occurs at the minimum output voltage $\upsilon_{O\min}$ as does the maximum output current $i_{O\max}$. The minimum load resistance of the ZCDS-CECS-RPFC $R_{L\min}$ is obtained as

$$R_{L\min} = \frac{\upsilon_{O\min}}{i_{O\max}} = \frac{V_B - V_{in}}{I_{in}}, \tag{1}$$

where $I_{O\max} = I_{in}$ is the output current flowing though the output voltage source υ_O. Moreover, the output voltage υ_O, the output current i_O, and the load resistance R_L of the ZCDS-CECS-RPFC vary with time at the frequency $2f_L$. From [46], the maximum duty ratio $D_{e\max}$ of the diode D_E of the ZCDS Class-E current-driven rectifier depends on the normalized load resistance $R_{L\min}/\omega_S L_E$ and can be written as

$$\frac{R_{L\min}}{\omega_S L_E} = \frac{2\pi}{1 - 2\pi^2 D_{e\max}^2 - \cos 2\pi D_{e\max} + \dfrac{(\sin 2\pi D_{e\max} - 2\pi D_{e\max})^2}{1 - \cos 2\pi D_{e\max}}} \tag{2}$$

The input power of the proposed single-stage LED driver is calculated as

$$P_{in} = \frac{V_{in} I_{in}}{2} = \frac{V_{in} I_{O\max}}{2} \tag{3}$$

Substituting this equation into (1) provides the relationship between the maximum duty ratio $D_{e\max}$ and the normalized load resistance of the ZCDS Class-E current-driven rectifier, as follows:

$$\frac{R_{L\min}}{\omega_S L_E} = \frac{\left(\frac{V_B}{V_{in}} - 1\right) V_{in}^{\;2}}{2 P_{in} \omega_S L_E}. \tag{4}$$

Combining (2) and (4), a voltage ratio between the DC-link voltage and the amplitude of the utility-line input voltage V_B/V_{in} of the ZCDS Class-E current-driven rectifier for the power-factor correction is

$$\frac{V_B}{V_{in}} = \frac{4\pi\omega_S L_E}{\left(1 - 2\pi^2 D_{e\max}^2 - \cos 2\pi D_{e\max} + \frac{(\sin 2\pi D_{e\max} - 2\pi D_{e\max})^2}{1 - \cos 2\pi D_{e\max}}\right) R_{L\min}} + 1 \tag{5}$$

The voltage ratio V_B/V_{in} was obtained from a simulation of the ZCDS Class-E current-driven rectifier at fixed values of the amplitude of the utility-line input voltage V_{in} = 311 V, the switching frequency f_S = 55 kH$_z$, and the parallel inductance L_E = 2.4 mH. Hence, the voltage ratio V_B/V_{in} is a function of the maximum duty ratio $D_{e\max}$ of the ZCDS Class-E current-driven rectifier as illustrated in Fig. 10. The duty ratio $D_e = D_{e\min} = 0$ at the no-load condition, and the duty ratio $D_e = D_{e\max}$ at the full-load condition. The numerical values of the ZCDS Class-E current-driven rectifier for the PFC parameters at selected maximum duty ratio values $D_{e\max}$ are given in Table III.

III. Design Procedure

The design of the proposed single-stage driver for the LED street-light modules can be divided into two parts: the PFC semi-stage and the driver semi-stage. The design steps of the PFC semi-stage are illustrated in Fig. 11, and the design procedures of the PFC semi-stage based on the ZCDS-CECS-RPFC are given as follows:

1) a near-sinusoidal utility-line input current was assumed, and an expected efficiency η was estimated. The amplitude of the utility-line input current I_{in}, which is the maximum output current $I_{O\max}$ of the ZCDS-CECS-RPFC, was obtained for a given input power P_{in}, output power P_{out}, and rms value of the utility-line input voltage $V_{in\mathrm{rms}}$.

2) select the maximum duty ratio $D_{e\max}$ from Table III according to the tradeoffs regarding the ratio of the DC-link voltage and the amplitude of the utility-line input voltage V_B/V_{in}. If a low value of the maximum duty ratio $D_{e\max}$ is selected, a low-total harmonic distortion of the line current (THD_i) is achieved, but the main switches have high-voltage stresses. If a high value of the maximum duty ratio $D_{e\max}$ is used, a high THD_i occurs, but the main switches have low-voltage stresses.

3) determine the DC-link voltage V_B from the specified utility-line input voltage V_{in} and add to a calculated the minimum load resistance $R_{L\min}$ of the ZCDS-CECS-RPFC.

4) find the parallel inductor L_E of the classic ZCDS Class-E rectifier, which is obtained from the normalized load resistance $R_{L\min}/\omega_S L_E$ at the same line as that of the chosen $D_{e\max}$ value in Table III.

5) find the full-load input impedance of the ZCDS Class-E current-driven rectifier Z_{isf}, which consists of the input resistance R_{isf} and the input reactance X_{isf} from Table III at the same line as that of the chosen $D_{e\max}$ value. The input resistance R_{is} and input reactance X_{is} are plotted versus D_e, as shown in Figs. 12 and 13, respectively.

6) find the amplitude of the equivalent voltage source υ_{eq} at the full-load condition.

7) calculate the amplitude of the driving current at full-load I_{eqf}.

8) find the no-load input impedance of the ZCDS Class-E current-driven rectifier Z_{isn}, which consists of the input resistance R_{isn} and input reactance X_{isn}.

9) find the amplitude of the equivalent voltage source υ_{eq} at the no-load condition.

10) calculate the amplitude of the driving current at the no-load condition I_{eqn}.

11) calculate the turn ratio n_{PFC} of the transformer T_1.

12) find the value of the inductance L_d from the results of procedures 5 to 11, with the assumption that the series inductance L_{dp} equals the primary inductance L_p of the transformer T_1.

13) find the value of inductance L_{dp} and add an additional inductance L_c to L_{dp} to cancel the reactance of the capacitance C_d.

A. PFC Semi-Stage Design

The single-stage LED driver for a 150-W LED street light was designed to handle a line rms voltage $V_{in\mathrm{rms}}$ of 220 V and a line frequency f_L of 50 H_z. It was assumed that the total efficiency η equaled 0.92 and the LED driver drew a sine-wave utility-line input current. The input power is obtained by

$$P_{in} = \frac{P_{out}}{\eta} \tag{6}$$

The amplitude of the utility-line input current I_{in}, which is the maximum output current $I_{O\max}$ of the ZCDS-CECS-RPFC, is given by

$$I_{in} = I_{O\max} = \frac{\sqrt{2}P_{in}}{V_{in\mathrm{rms}}} \tag{7}$$

The maximum duty ratio $D_{e\max} = 0.9$ was used because it gives the best compromise between the THD_i and reasonable value of the voltage stress of the power switches M_1-M_2. From Table III, we achieved the following: $V_B/V_{in} = 1.0932$, the amplitude of the utility-line input voltage $V_{in} = \sqrt{2}V_{in\mathrm{rms}} \approx 311\,\mathrm{V}$ and the DC-link voltage $V_B \approx 340$ V. Substitute these values into equation (1) to obtain the full-load resistance of the ZCDS-CECS-RPFC, which is $R_{L\min}$. The parallel inductance L_E of the ZCDS Class-E current-driven rectifier can be obtained from the normalized load resistance $R_{L\min}/\omega_S L_E$ at the same line as that of the chosen $D_{e\max}$ value in Table III.

$$L_E = \frac{R_{L\min}}{0.0334\omega_S}, \tag{8}$$

where the switching frequency $f_S = 55$ kH$_z$. At the full-load condition, the input impedance of the ZCDS Class-E current-driven rectifier is as follows:

$$Z_{isf} = R_{isf} + jX_{isf}, \tag{9}$$

where

$$R_{isf} = 0.0560\omega_S L_E \tag{10}$$

and

$$X_{isf} = 0.0228\omega_S L_E \tag{11}$$

The amplitude of the driving current at full-load condition I_{eqf} is calculated from

$$I_{eqf} = \sqrt{\frac{2I_{O\max}(V_B - V_{in})}{R_{isf}}} \tag{12}$$

The amplitude of the equivalent voltage source V_{eq} at the full-load condition is given by

$$V_{eq} = I_{eqf}\sqrt{R_{isf}^2 + \left(\omega_S L_{isf} + \omega_S L_{eq}\right)^2} \tag{13}$$

At the no-load condition, the input impedance of the ZCDS Class-E current-driven rectifier is

$$Z_{isn} = R_{isn} + jX_{isn} \tag{14}$$

The inductance L_{isn} equals the inductance L_E. The amplitude of the driving current under the no-load condition I_{eqn} is obtained by

$$I_{eqn} = \frac{V_B}{\left|j\omega_S L_E\right|} \tag{15}$$

The amplitude of the equivalent voltage source V_{eq} under the no-load condition is calculated by

$$V_{eq} = I_{eqn}\left|j\omega_S L_{eq} + j\omega_S L_{isn}\right| \tag{16}$$

The values of V_{eq} and L_{eq} are obtained by solving (13) and (16). The turn ratio n_{PFC} of the transformer T_1 is determined by

$$n_{PFC} = \frac{\pi V_{eq}}{V_B} \tag{17}$$

To simplify the design procedure, assume that the series inductance L_{dp} equals the primary inductance L_p of the transformer T_1. Consequently, the driven inductance L_{dp} is given by

$$L_{dp} = \frac{2L_{eq}}{n_{PFC}^2} \tag{18}$$

For a finite value of a capacitance C_d, an additional L_c can be added to the inductance L_{dp} to compensate for the reactance of a capacitance C_d. The value of the additional inductance L_c is determined by

$$L_c = \frac{1}{\omega_S^2 C_d} \tag{19}$$

Therefore, the total inductance L_{dc} is

$$L_{dc} = L_{dp} + L_c \tag{20}$$

To achieve a ripple voltage of less than 1%, the value of the DC-link capacitor is determined by

$$C_B = \frac{P_{in}}{0.02 V_B^2 \omega_L} \tag{21}$$

Normally, the DC-link capacitance C_B and the output capacitance C_O should be larger to accommodate a high LED current ripple, which may influence the lighting quality [47]. If low capacitances are selected, a high LED current ripple occurs. Alternatively, if high capacitances are used, a low LED current ripple occurs. For long lifespan applications, high-temperature electrolytic capacitors are adequate for the DC-link capacitor C_B and the output capacitor C_O for low cost LED drivers and are widely used in the market. According to the lifespan estimation method of the electrolytic capacitor [48]–[50], the lifespan of the high temperature electrolytic capacitors doubles for every 10 °C decrease of the operating temperature below the rated level.

B. Losses Analysis

The circuit losses of the presented single-stage LED driver for an LED street light can be divided into five major components, which are the power diodes, the power MOSFETs, the inductors, the transformers, and the sensing resistor. The simple equivalent circuit for a conduction loss analysis is shown in Fig. 8(b). For The bridge-rectifier D_1-D_4 was built using standard recovery diodes. The average value of the input rectifier diode currents i_{D1}-i_{D4} equals the average value of the half-wave rectified utility-line input current. Thus, the diode losses in one diode of the bridge-rectifier diode are calculated from

$$P_{DB} = \frac{V_{FDB} I_{in}}{\pi} + \frac{I_{in}^2 R_{FDB}}{4}, \qquad (22)$$

where V_{FDB} is the diode threshold voltage, and R_{FDB} is the diode forward resistance of the bridge-rectifier diode. The ZCDS Class-E current-driven rectifier was built using a silicon carbide Schottky diode D_E. The power loss in the diode D_E is determined using

$$P_{DE} = \frac{2V_{FDE} I_{in}}{\pi} + \frac{I_{in}^2 R_{FDE}}{2}, \qquad (23)$$

where V_{FDE} is the diode threshold voltage, and R_{FDE} is the diode forward resistance of the ZCDS Class-E current-driven rectifier diode. The full-wave center-tapped rectifier of the ZVS Class-D *LLC* resonant converter was built using two silicon Schottky diodes D_{D1}-D_{D2}. The conduction losses in each diode are obtained using

$$P_{DD} = \frac{V_{FDD} I_{LED}}{2} + \frac{\pi I_{LED}^2 R_{FDD}}{16}, \qquad (24)$$

where V_{FDD} is the diode-threshold voltage, and R_{FDD} is the diode forward resistance of these silicon Schottky diodes. For the power switches M_1 and M_2, the turn-on switching losses are both zero; thus, the losses of the power switches are composed of the conduction losses and turn-off switching losses, which can be determined using

$$P_{DS} = I_{s\mathrm{rms}}^2 r_{DS(\mathrm{on})} + \left(\frac{V_B I_M t_r}{3T_S} + \frac{V_B I_M t_f}{2T_S} \right), \qquad (25)$$

where $r_{DS(\mathrm{on})}$ represents the resistance when the power MOSFET is turned on and t_r and t_f are the switch-voltage rise time and switch-current fall time of the power switches M_1 and M_2 during turn-off, respectively. The rms values of the drain current of the power MOSFET is determined by

$$I_{s\mathrm{rms}} = \sqrt{I_{dp\mathrm{rms}}^2 + I_{r\mathrm{rms}}^2} \qquad (26)$$

The rms value of the driving current $I_{dp\text{rms}}$ of the ZCDS-CECS-RPFC can be obtained using the principle of double side band amplitude modulation (DSB-AM) with a carrier signal [51] and is given by

$$I_{dp\text{rms}} = \frac{n_{PFC}\left(I_{eqf} + 2I_{eqn}\right)\sqrt{2+m^2}}{4}, \tag{27}$$

where m is the ratio between the modulated and unmodulated carrier amplitudes. In the case of the ZCDS-CECS-RPFC, the modulation index $m = 0.33$. From Fig. 8(c) the rms values of the drain current of the power MOSFETs are the sum of the rms values of the driving current i_{dp} and the resonant current i_r. The rms value of the resonant current in the ZVS Class-D LLC resonant converter semi-stage $I_{r\text{rms}}$ [44], [45] can be obtained as

$$I_{r\text{rms}} = \frac{1}{\eta_c}\sqrt{\left(\frac{\pi I_{LED}}{n_{LLC}\sqrt{8}}\right)^2 + \left(\frac{n_{LLC}\left(V_{LED} + V_{FDD}\right)}{4\sqrt{2} f_S M_V \left(L_{mD} - L_r\right)}\right)^2} \tag{28}$$

It was assumed that the ZVS Class-D LLC resonant converter efficiency $\eta_c = 0.95$, the turn ratio of the transformer T_2 $n_{LLC} = 6$, and the DC to DC voltage transfer function $M_V = 1.12$. The losses of the magnetic components can be separated into the core loss and the copper loss. Therefore, the core losses in the EMI filter inductor L_f, the series inductor L_{dc}, and the transformers T_1, T_2 can be obtained using the improved generalized Steinmetz equation [52]–[54]

$$P_{\text{core}} = \frac{1}{T_s}\int_0^{T_S}\left(\frac{k}{(2\pi)^{\alpha-1}\int_0^{2\pi}\left|\cos\theta\right|^{\alpha} 2^{\beta-\alpha}\, d\theta} \left|\frac{dB}{dt}\right|^{\alpha} (\Delta B)^{\beta-\alpha}\, dt\right), \tag{29}$$

where k is a core loss coefficient, α is a frequency exponent, β is a core loss exponent, and B is a peak to peak value of an induction sinusoidal waveform. The copper resistance of the EMI filter inductor is r_{Lf} and the rms value of the current flowing through the winding of the EMI filter inductor i_{Lf} equals the rms value of the full-wave rectified utility-line input current. Hence, the copper loss in the EMI filter inductor is calculated by

$$P_{rLf} = \frac{I_{in}^2 r_{Lf}}{2} \quad (30)$$

The copper loss in the series inductor P_{rLdc} is obtained by

$$P_{rLdc} = I_{dp\mathrm{rms}}^2 r_{Ldc}\,, \quad (31)$$

where r_{Ldc} represented the equivalent series resistance (ESR) of the series inductor L_{dc}. The copper losses of the transformer T_1 can be divided into the primary side and the secondary side. The copper loss in the winding of the primary side r_{pT1} of the transformer T_1 is calculated by

$$P_{rpT1} = I_{dp\mathrm{rms}}^2 r_{pT1} \quad (32)$$

The rms value of the current flowing through the winding of the secondary side r_{sT1} of the transformer T_1 equals the rms value of the full-wave rectified utility-line input current. Therefore, the copper loss in the winding of the secondary side r_{sT1} of the transformer T_1 is given by

$$P_{rsT1} = \frac{I_{in}^2 r_{sT1}}{2} \quad (33)$$

The copper loss in the winding of the primary side r_{pT2} of the transformer T_2 is calculated from

$$P_{rpT2} = I_{r\mathrm{rms}}^2 r_{pT2} \quad (34)$$

The copper loss in the winding of the secondary side r_{sT2} of the transformer T_2 is given by

$$P_{rsT2} = \frac{r_{sT2}\pi^2 I_{LED}^2}{16} \quad (35)$$

By using Ohm's law, the current sensing resistor R_{sense} can be expressed as

$$R_{sense} = \frac{V_{csth}}{I_{LED\max}}, \tag{36}$$

where V_{csth} is the current sense threshold, and $I_{LED\max}$ is the maximum output current. Therefore, the power loss of the current sensing resistor R_{sense} can be calculated by

$$P_{Rsense} = I_{LED\max}^2 R_{sense} \tag{37}$$

The total loss of the proposed single-stage LED driver P_l is given by

$$\begin{aligned} P_l = {} & 2P_{DB} + P_{DE} + 2P_{DD} + 2P_{DS} + P_{\mathrm{core}} + P_{rLf} \\ & + P_{rLdc} + P_{rpT1} + P_{rsT1} + P_{rpT2} + P_{rsT2} + P_{Rsense} \end{aligned} \tag{38}$$

The efficiency of the presented single-stage LED driver η is given by

$$\eta = \frac{P_{out}}{P_{in}} \times 100\% = \frac{P_{out}}{P_{out} + P_l} \times 100\% \tag{39}$$

The 150-W LED street-light driver is constructed from 3 modules of the 50-W/32-V LED module connected in parallel, as shown in Fig. 9(d). The design of the ZVS Class-D *LLC* resonant converter can be found in references [40]–[45], and the design of the EMI filter can be found in reference [55].

IV. Experimental Results

To verify the theoretical analysis, the prototype of the proposed single-stage LED driver was built using the prototype parameters obtained from the design procedure given previously and listed in Table IV. The prototype of the proposed single-stage LED driver based on the ZCDS-CECS-RPFC is depicted in Fig. 14. The utility-line input voltage is set to 220 V_{rms} with a frequency f_L of 50 H_z. The measured waveforms of the utility-line input voltage v_{in} and the current i_{in} at full power are displayed in Fig. 15. The shape of utility-line input current is sinusoidal and in phase with the utility-line input voltage. At the rated output power of 150 W, the input power that was measured using a power analyzer model 43B (FLUKE) was 164 W, and the PF was 0.99. The THD_i was 7.9%, as shown in Fig. 16.

To measure the key circuit waveforms, a mixed signal oscilloscope (model DL2024), a differential probe (model 700924), and a current probe (model 701932) that were manufactured by YOKOGAWA were employed. The measured waveform of the driving current i_{dp} with a zoomed-in view near the peak of the utility-line input voltage is shown in Fig. 17. It can be seen that the amplitude of the driving current i_{dp} near the zero crossing of the utility-line input voltage is low. As a result, the current stresses of the power MOSFETs have been significantly reduced when compared to the ZVDS-CECS-RPFC [34] and ZVDS-CDECS-RPFC [35] topologies.

The switch voltage υ_E and the switch current i_E waveforms of D_E of the ZCDS Class-E current-driven rectifier at 60 degrees of the utility-line input voltage are shown in Fig. 18. The result shows that the diode D_E turns on at zero di/dt and low $d\upsilon/dt$, which allows the high-efficiency and low-switching noise to be captured.

Figs. 19(a) and (b) present the measured waveforms of the diode voltage υ_E and the diode current i_E of the ZCDS-CECS-RPFC near the peak and the zero-crossing of the utility-line input voltage, respectively. The experimental results of the rectified utility-line input voltage $|\upsilon_{in}|$, the combined voltage waveform $\upsilon_O = V_B - |\upsilon_{in}|$, and the rectified utility-line input current $|i_{in}|$ are shown in Fig. 20. As expected, the current of the diode D_E increased, and the combined voltage υ_O decreased as the instantaneous utility-line input voltage increased; conversely, the current of the diode D_E decreased, and the combined voltage υ_O increased as the instantaneous utility-line input voltage decreased. These waveforms roughly match the required waveforms illustrated in Fig. 6. Figs. 21(a) and (b) illustrate the experimental waveforms of the switch voltage and the switch current of the power MOSFETs M_1 and M_2 near the peak and the zero-crossing of the utility-line input voltage, respectively. The maximum voltage stresses of switch M_1 and M_2 were both approximately 340 V, and ZVS can be achieved.

Fig. 22 presents the experimental waveforms of the utility-line input voltage (Ch1), the utility-line input current (Ch2), the input power (Math1), het output voltage (Ch3), the output current (Ch4) and the output power (Math2). The input power P_{in} was 164.372 W, and the output power P_{out} was 150.285 W. Hence, the measured system efficiency of the single-stage LED driver η under the full output power and a fixed value of the utility-line input voltage $V_{in\mathrm{rms}}$ = 220 V was approximately 91.4%. As expected, the proposed topology is more efficient because the ZVDS-CECS-RPFC [34] and ZVDS-CDECS-RPFC [35] topologies had more high-current stress in the PFC semi-stage. It can be observed that the measured LED current ripple was approximately 18% of I_{LED}. According to [47], this value is well below the acceptable limits of flicker and the perception of stroboscopic effects.

Figs. 23(a) and (b) depict the measured system PF and THD_i of the proposed topology under the utility-line input voltage range of 180 V_{rms} to 250 V_{rms} at P_{out} = 150 W and the different output power range of 60 W to 150 W at υ_{in} = 220 V_{rms}, respectively. It can be observed that the PF is always higher than 0.97, and the THD_i is lower than 20%. Table V shows the measured utility-line input-current harmonic contents, under the two-level output powers of 60 W and 150 W, compared with the IEC 61000-3-2 Class-C at the nominal utility-line input voltage of 220 V_{rms}. The results completely meet the power-factor requirement and the utility-line input current harmonic contents of the lighting equipment standard IEC 61000-3-2 Class-C.

The main losses come from the conduction losses in the PFC semi-stage elements, such as the ESR of the series inductor L_{dc}, the copper resistance of the transformer T_1 and the power switches M_1 and M_2. It can be seen that the system efficiency has been reduced when operated from the low utility-line input voltage because the higher driving current i_d. Therefore, the proposed single-stage LED driver based on the ZCDS-CECS-RPFC has to be designed with only ±15% of the standard utility-line input voltages of 220 V_{rms} or 110 V_{rms}, respectively, and is not suitable for universal-line voltages, which are in the range of 90 V_{rms} to 265 V_{rms}. The system efficiency when the utility-line input voltage changes from 180 V_{rms} to 250 V_{rms} at full-load and the output power varies from 60 W to 150 W at 220 V_{rms} is illustrated in Figs. 24(a) and (b), respectively.

Additionally, Table VI shows the component count and key performance comparison of the ZVDS-CECS-RPFC [34], the ZVDS-CDECS-RPFC [35], the ZCS-CDCS-RPFC [38], and the proposed ZCDS-CECS-RPFC. The proposed LED driver has a good system efficiency compared with the previous ZVS-RPFC topologies and a low THD_i when compared with the previous ZCS-RPFC topologies. The comparative study of the proposed ZCDS-CECS-RPFC with the previously LED street-light drivers that employ two-stage topologies is depicted in Table VII. It can be seen that the two-stage LED drivers have many power switches and controller ICs for each stage, which leads to high costs, complexity and large sizes.

V. Discussion of the Effect of Junction Capacitance of the ZCDS-CECS-RPFC Diode

To achieve the low-total harmonic distortion of the utility-line input current, the utility-line input current i_{in} near the zero-crossing of the utility-line input voltage must equal zero. The utility-line input current i_{in} cannot reach zero near the utility-line input voltage υ_{in}, due to the junction capacitance effect of the ZCDS Class-E current-driven rectifier diode D_E, as shown in Fig. 25(a). In this circuit, the equivalent circuit cannot be modeled by a series combination of the inductor L_{ds} with the input impedance of the ZCDS Class-E current-driven rectifier. In a first simplified approach, the voltage source υ_O appears as a short circuit to the high-frequency AC component and the junction capacitor C_j is interchangeable. Therefore, the input impedance of the ZCDS Class-E current-driven rectifier with the parasitic capacitance effect can be modeled by the parallel L_{sp}-R_{sp} or the series L_{ss}-R_{ss} with the junction capacitor C_j as presented in Figs. 25(b) and (c), respectively. It is well known that the voltage transfer function of the *LLC* resonant inverter is more than 1 [43]. Thus, near the zero-crossing of the utility-line input voltage υ_{in}, the D_E can conduct current because the voltage at its anode is more positive than the voltage at its cathode. As a result, the utility-line input current i_{in} cannot reach zero. Accordingly, a diode with a small C_j is preferred.

VI. Conclusion

This paper has proposed a circuit of a single-stage LED driver for street-lighting applications. The LED driver combines a modified zero-current and zero-derivative-switching Class-E current-driven rectifier as a power-factor correction semi-stage with a zero-voltage-switching Class-D *LLC* resonant converter as a driver semi-stage into one power-conversion stage. A 150-W experimental prototype LED driver has been developed and tested with the utility-line input voltages ranging from 180~250 V_{rms}/50 H_z. The experimental results of the single-stage LED driver prototype had a high PF (0.99), a low THD_i (7.9%), and high system efficiency (91.4%) at rated load condition. The THD_i of the proposed LED driver was lower than the ZCS-RPFC topologies, while the system efficiency was higher than that of the ZVS-RPFC topologies, due to the reduced current stresses in the power MOSFETs near the zero-crossing of the utility-line input voltage. The power MOSFETs can be operated under the ZVS condition and the diode in the PFC semi-stage turns on at zero *di/dt* and low *dυ/dt*. Therefore, a low-switching noise level can be achieved.

References

[1] K. I. Hwu and Y. T. Yau, "Applying one-comparator counter-based sampling to current sharing control of multichannel LED strings," *IEEE Trans. Industry Applications*, vol. 47, no. 6, pp. 2413–2421, Nov./Dec. 2011.

[2] M. K. Kazimierczuk and W. Szaraniec, "Electronic ballast for fluorescent lamps," *IEEE Trans. on Power Electronics*, vol. 8, no. 4, pp. 386–395, Oct. 1993.

[3] M. Arias, D. G. Lamar, F. F. Linera, D. Balocco, A. A. Diallo, and J. Sebastian, "Design of a soft-switching asymmetrical half-bridge converter as second stage of an LED driver for street lighting application," *IEEE Trans. Power Electronics*, vol. 27, no. 3, pp. 1608–1697, Mar. 2012.

[4] M. Arias, D. G. Lamar, J. Sebastian, D. Balocco, and A. A. Diallo, "High-efficiency LED driver without electrolytic capacitor for street lighting," *IEEE Trans. Industry Applications*, vol. 49, no. 1, pp. 127–137, Jan./Feb. 2013.

[5] M. Arias, M. F. Diaz, D. G. Lamar, D. Balocco, A. A. Diallo, and J. Sebastian, "High-efficiency asymmetrical half-bridge converter without electrolytic capacitor for low-output-voltage AC–DC LED drivers," *IEEE Trans. Power Electronics*, vol. 28, no. 5, pp. 2539–2550, May 2013.

[6] J. Garcia, M. A. D. Costa, A. L. Kirsten, D. Gacio, and A. J. Calleja, "A novel flyback-based input PFC stage for electronic ballasts in lighting applications," *IEEE Trans. Industry Applications*, vol. 49, no. 2, pp. 769–777, Mar./Apr. 2013.

[7] F. Zhang, J. Ni, and Y. Yu, "High power factor AC-DC LED driver with film capacitors," *IEEE Trans. Power Electronics*, vol. 28, no. 10, pp. 4831–4840, Oct. 2013.

[8] Y. C. Shen, T. J. Liang, W. J. Tseng, H. H. Chang, K. H. Chen, Y. J. Lu, and J. S. Li, "Non-electrolytic capacitor LED driver with feed forward control," *IEEE Energy Conversion Congress and Exposition*, pp. 3223–3230, Sep. 2015.

[9] Y. Wang, Y. Guan, D. Xu, and W. Wang, "A *CLCL* resonant DC/DC converter for two-stage LED driver system," *IEEE Trans. Industrial Electronics*, vol. 63, no. 5, pp. 2883–2891, May 2016.

[10] J. Zhang, T. Jiang, and X. Wu, "A high-efficiency quasi-two-stage LED driver with multichannel outputs," *IEEE Trans. Industrial Electronics*, vol. 64, no. 7, pp. 5875–5882, Jul. 2017.

[11] Y. Hu, L. Huber, and M. M. Jovanovic, "Single-stage, universal-input AC/DC LED driver with current-controlled variable PFC boost inductor," *IEEE Trans. on Power Electronics*, vol. 27, no. 3, pp. 1579–1588, Mar. 2012.

[12] P. Fang, B. White, C. Fiorentino, and Y. F. Liu, "Zero ripple single stage AC-DC LED driver with unity power factor," *IEEE Energy Conversion Congress and Exposition*, pp. 3452–3458, Sep. 2013.

[13] Y. C. Li and C. L. Chen, "A novel primary-side regulation scheme for single-stage high-power-factor AC–DC LED driving circuit," *IEEE Trans. Industrial Electronics*, vol. 60, no. 11, pp. 4978–4986, Nov. 2013.

[14] X. Xie, J. Li, K. Peng, C. Zhao, and Q. Lu, "Study on the single-stage forward-flyback PFC converter with QR control," *IEEE Trans. Power Electronics*, vol. 31, no. 1, pp. 430–442, Jan. 2016.

[15] Y. Wang, J. Huang, W. Wang, and D. Xu, "A single-stage single-switch LED driver based on Class-E converter," *IEEE Trans. Industry Applications*, vol. 52, no. 3, pp. 2618–2626, May/Jun. 2016.

[16] Y. Wang, J. Huang, G. Shi, W. Wang, and D. Xu, "A single-stage single-switch LED driver based on the integrated SEPIC circuit and Class-E converter," *IEEE Trans. Power Electronics*, vol. 31, no. 8, pp. 5814–5824, Aug. 2016.

[17] Y. Guo, S. Li, A. T. L. Lee, S. C. Tan, C. K. Lee, and S. Y. R. Hui, "Single-stage AC/DC single-inductor multiple-output LED drivers," *IEEE Trans. on Power Electronics*, vol. 31, no. 8, pp. 5837–5850, Aug. 2016.

[18] X. Liu, Q. Yang, Q. Zhou, J. Xu, and G. Zhou, "Single-stage single-switch four-output resonant LED driver with high power factor and passive current balancing," *IEEE Trans. Power Electronics*, vol. 32, no. 6, pp. 4566–4576, Jun. 2017.

[19] P. Fang, Y. J. Qiu, H. Wang, and Y. F. Liu, "A single-stage primary-side-controlled off-line flyback LED driver with ripple cancellation," *IEEE Trans. Power Electronics*, vol. 32, no. 6, pp. 4700–4715, Jun. 2017.

[20] Q. Luo, J. Huang, Q. He, K. Ma, and L. Zhou, "Analysis and design of a single-stage isolated AC-DC LED driver with a voltage doubler rectifier," *IEEE Trans. Industrial Electronics*, vol. 64, no. 7, pp. 5807–5817, Jul. 2017.

[21] B. Poorali, E. Adib, and H. Farzanehfard, "A single-stage single-switch soft-switching power-factor-correction LED driver," *IEEE Trans. Power Electronics*, vol. 32, no. 10, pp. 7932–7940, Oct. 2017.

[22] C. A. Cheng, H. L. Cheng, and T. Y. Chung, "A novel single-stage high-power-factor LED street-lighting driver with coupled inductors," *IEEE Trans. Industry Applications*, vol. 50, no. 5, pp. 3037–3045, Sep./Oct. 2014.

[23] H. L. Cheng and C. W. Lin, "Design and implementation of a high-power-factor LED driver with zero-voltage switching-on characteristics," *IEEE Trans. Power Electronics*, vol. 29, no. 9, pp. 4949–4958, Sep. 2014.

[24] C. A. Cheng, C. H. Chang, T. Y. Chung, and F. L. Yang, "Design and implementation of a single-stage driver for supplying an LED street-light module with power factor corrections," *IEEE Trans. Power Electronics*, vol. 30, no. 2, pp. 956–966, Feb. 2015.

[25] Y. Wang, Y. Guan, K. Ren, W. Wang, and D. Xu, "A single-stage LED driver based on BCM boost circuit and *LLC* converter for street lighting system," *IEEE Trans. Industrial Electronics*, vol. 62, no. 9, pp. 5446–5457, Sep. 2015.

[26] U. R. Reddy and B. L. Narasimharaju, "Single-stage electrolytic capacitor less non-inverting buck-boost PFC based AC–DC ripple free LED driver," *IET Power Electronics*, vol. 10, no. 1, pp. 38–46, Jan. 2016.

[27] H. Ma, J. S. Lai, C. Zheng, and P. Sun, "A high-efficiency quasi-single-stage bridgeless electrolytic capacitor-free high-power AC-DC driver for supplying multiple LED strings in parallel," *IEEE Trans. Power Electronics*, vol. 31, no. 8, pp. 5825–5836, Aug. 2016.

[28] J. M. Alonso, J. Vina, D. G. Vaquero, G. Martinez, and R. Osorio, "Analysis and design of the integrated double buck–boost converter as a high-power-factor driver for power-LED lamps," *IEEE Trans. Industrial Electronics*, vol. 59, no. 4, pp. 1689–1697, Apr. 2012.

[29] Z. P. da Fonseca, A. J. Perin, E. A. Junior, and C. B. Nascimento, "Single-stage high power factor converters requiring low DC-link capacitance to drive power LEDs," *IEEE Trans. Industrial Electronics*, vol. 64, no. 5, pp. 3557–3567, May 2017.

[30] Q. Luo, K. Ma, Q. He, C. Zou, and L. Zhou, "A single-stage high-frequency resonant AC/AC converter," *IEEE Trans. Power Electronics*, vol. 32, no. 3, pp. 2155–2166, Mar. 2017.

[31] G. G. Pereira, M. A. D. Costa, J. M. Alonso, M. F. D. Melo, and C. H. Barriquello, "LED driver based on input current shaper without electrolytic capacitor," *IEEE Trans. Industrial Electronics*, vol. 64, no. 6, pp. 4520–4529, Jun. 2017.

[32] Y. Wang, N. Qi, Y. Guan, C. Cecati, and D. Xu, "A single-stage LED driver based on SEPIC and *LLC* circuits," *IEEE Trans. Industrial Electronics*, vol. 64, no. 7, pp. 5766–5776, Jul. 2017.

[33] H. Ma, G. Chen, J. H. Yi, Q. W. Meng, L. Zhang, and J. P. Xu, "A single-stage PFM-APWM hybrid modulated soft-switched converter with low bus voltage for high-power LED lighting applications," *IEEE Trans. Industrial Electronics*, vol. 64, no. 7, pp. 5777–5788, Jul. 2017.

[34] K. Jirasereeamornkul, M. K. Kazimierczuk, I. Boonyaroonate, and K. Chamnongthai, "Single-stage electronic ballast with Class-E rectifier as power-factor corrector," *IEEE Trans. Circuits and Systems* I, vol. 53, no. 1, pp. 139–148, Jan. 2006.

[35] C. Ekkaravarodome, A. Nathakaranakule, and I. Boonyaroonate, "Single-stage electronic ballast using Class-DE low-*dυ/dt* current-source driven rectifier for power-factor correction," *IEEE Trans. Industrial Electronics*, vol. 57, no. 10, pp. 3405–3414, Oct. 2010.

[36] C. Ekkaravarodome and K. Jirasereeamornkul, "Single-stage high-power-factor electronic ballast with a symmetrical Class-DE resonant rectifier," *Journal of Power Electronics,* vol. 12, no. 3, pp. 429–438, May/Jun. 2012.

[37] C. Ekkaravarodome, K. Jirasereeamornkul, and M. K. Kazimierczuk, "Implementation of a DC-side Class-DE low-*dυ/dt* rectifier as a PFC for electronic ballast application," *IEEE Trans. Power Electronics*, vol. 29, no. 10, pp. 5486–5497, Oct. 2014.

[38] C. Ekkaravarodome, V. Chunkag, K. Jirasereeamornkul, and M. K. Kazimierczuk, "Class-D zero-current-switching rectifier as power-factor corrector for lighting applications," *IEEE Trans. Power Electronics*, vol. 29, no. 9, pp. 4938–4948, Sep. 2014.

[39] C. Ekkaravarodome, P. Thounthong, K. Jirasereeamornkul, and K. Higuchi, “Analysis and design of DC-side symmetrical Class-D ZCS rectifier as PFC for lighting applications,” *Journal of Power Electronics,* vol. 15, no. 3, pp. 621–633, May/Jun. 2015.

[40] M. K. Kazimierczuk and X. T. Bui, “Class E dc/dc converters with an inductive impedance inverter,” *IEEE Trans. Power Electronics*, vol. PE-4, no. 1, pp. 124–135, Jan. 1989.

[41] D. Czarkowski and M. K. Kazimierczuk, “Phase-controlled *CLL* resonant converter,” *Proceedings of the IEEE Applied Power Electronics Conference*, San Diego, CA, pp. 432–438, Mar. 7–11, 1993.

[42] M. K. Kazimierczuk and N. Thirunarayan, “Class D voltage-switching inverter with tapped resonant inductor,” *IEE Proceedings, Pt. B., Electric Power Applications*, vol. 140, pp. 177–185, May 1993.

[43] M. K. Kazimierczuk and D. Czarkowski, *Resonant Power Converters*, 2nd Ed, IEEE Press and John Wiley & Sons, New York, NY, 2011, chs. 6, 9 and 18.

[44] W. Feng, F. C. Fred, and P. Mattavelli, “Optimal trajectory control of burst mode for *LLC* resonant converter,” *IEEE Trans. Power Electronics*, vol. 28, no. 1, pp. 457–466, Jan. 2013.

[45] “Half-bridge *LLC* resonant converter design using FSFR-series Fairchild power switch,” Fairchild Semiconductor Corporation, California, United States, Oct. 2014.

[46] M. K. Kazimierczuk and J. Jozwik, “Analysis and design of Class E zero-current-switching rectifier,” *IEEE Trans. Circuits and Systems*, vol. 37, no. 8, pp. 1000–1009, Aug. 1990.

[47] P. S. Almeida, V. C. Bender, H. A. C. Braga, M. A. D. Costa, T. B. Marchesan, and J. M. Alonso, “Static and dynamic photoelectrothermal modeling of LED lamps including low-frequency current ripple effects,” *IEEE Trans. Power Electronics*, vol. 30, no. 7, pp. 3841–3851, Jul. 2015.

[48] Nippon Chemi-Con Corporation, “Judicious use of aluminum electrolytic capacitors,” *Technical notes*, pp. 1–14, Tokyo, Japan, 2012.

[49] P. S. Almeida, D. Camponogara, M. D. Costa, H. Braga, and J. M. Alonso, “Matching LED and driver life spans: a review of different techniques,” *IEEE Industrial Electronics Mag*., vol. 9, no. 2, pp. 36–47, Jun. 2015.

[50] B. Sun, X. Fan, C. Qian, and G. Zhang, “PoF-simulation-assisted reliability prediction for electrolytic capacitor in LED drivers,” *IEEE Trans. Industrial Electronics*, vol. 63, no. 11, pp. 6726–6735, Nov. 2016.

[51] L. E. Frenzel, *Principles of Electronic Communication Systems*, 3rd Ed, McGraw-Hill, New York, NY, 2008.

[52] A. V. den Bossche and V. C. Valchev, *Inductors and Transformers for Power Electronics*, CRC Press and Taylor & Francis, Boca Raton, FL, 2005, ch. 3.

[53] J. Muhlethaler; J. Biela, J. W. Kolar, and A. Ecklebe “Improved core-loss calculation for magnetic components employed in power electronic systems,” *IEEE Trans. Power Electronics*, vol. 27, no. 2, pp. 964–973, Feb. 2012.

[54] M. K. Kazimierczuk, *High-Frequency Magnetic Components*, 2nd Ed, John Wiley & Sons, Chichester, UK, 2013, ch. 2.

[55] V. Vlatkovic, D. Borojevic, and F. C. Lee, “Input filter design for power factor correction circuits,” *IEEE Trans. Power Electronics*, vol. 11, no. 2, pp. 199–205, Jan. 1996.

Figure captions

Fig. 1. Generic structure of LED drivers: (a) Two-stage LED drivers. (b) Single-stage LED drivers.

Fig. 2. Family of RPFC topologies.

Fig. 3. Conceptual diagram of the proposed single-stage LED driver based on a ZCDS-CECS-RPFC.

Fig. 4. Circuit configuration of a ZCDS-CECS-RPFC for a single-stage LED driver with an output voltage and current controls.

Fig. 5. Circuit derivation of the PFC with a ZCDS Class-E current-driven rectifier during the positive utility-line input half-cycle: (a) Equivalent circuit. (b) Equivalent circuit with the magnetizing inductance reflected from the primary side of the transformer T_1. (c) Equivalent circuit with the sine-wave voltage source υ_s and the series inductor L_{ds} reflected from the primary side of the transformer T_1. (d) Equivalent circuit with the high-frequency current source i_{ds}. (e) Equivalent circuit with combined voltage source $\upsilon_O = V_B - |\upsilon_{in}|$.

Fig. 6. Conceptual waveforms of the ZCDS-CECS-RPFC: (a) Utility-line input voltage υ_{in} waveform. (b) Rectified utility-line input voltage $|\upsilon_{in}|$ waveform. (c) Combined voltage $V_B - |\upsilon_{in}|$ waveform. (d) High-frequency driven current i_{dp} waveform. (e) Current i_s waveform of equivalent square-wave voltage source υ_{DS2}. (f) Diode current i_E waveform of the ZCDS-CECS-RPFC. (g) Utility-line input current waveform i_{in} is the filtered average diode current of the ZCDS-CECS-RPFC.

Fig. 7. Theoretical current and voltage waveforms of the proposed LED driver during one switching cycle.

Fig. 8. Circuit of the ZCDS Class-E rectifier semi-stage and the ZVS Class-D *LLC* resonant converter: (a) Circuit with the ZCDS Class-E current-driven rectifier and a series circuit. (b) The ZCDS Class-E current-driven rectifier is replaced by the primary equivalent circuit L_{ip}-R_{ip}, and the ZVS Class-D *LLC* resonant converter is transformed into an AC-equivalent circuit. (c) AC-equivalent circuit of the proposed single-stage LED driver.

Fig. 9. Simplified equivalent circuits of the proposed single-stage LED driver: (a) A ZCDS-CECS-RPFC with an equivalent sine-wave voltage source. (b) Components from the primary side of T_1 reflected to the secondary side. (c) AC-equivalent circuit of the PFC semi-stage. (d) AC-equivalent circuit of the LED driver semi-stage.

Fig. 10. Voltage ratio between DC-link voltage and the amplitude of the utility-line input voltage V_B/V_{in} as a function of D_e.

Fig. 11. Design steps of PFC semi-stage based on the ZCDS-CECS-RPFC.

Fig. 12. Normalized input resistance of the ZCDS-CECS-RPFC $R_{is}/\omega_S L_E$ as a function of D_e.

Fig. 13. Normalized input reactance of the ZCDS-CECS-RPFC $X_{is}/\omega_S L_E$ as a function of D_e.

Fig. 14. Prototype photograph of the proposed single-stage 150-W LED driver based on the ZCDS-CECS-RPFC.

Fig. 15. Experimental utility-line input voltage and current waveforms.

Fig. 16. Measured value of the utility-line input current THD_i.

Fig. 17. Measured driving current i_{dp} waveform; lower waveform is a zoomed-in view of the top waveform near the peak of the utility-line input voltage.

Fig. 18. Experimental waveforms of the diode voltage υ_E and the current i_E of the ZCDS-CECS-RPFC at 60 degrees of the utility-line input voltage.

Fig. 19. Experimental rectifier diode voltage υ_E and current i_E waveforms: (a) Near the peak of the utility-line input voltage. (b) Near the zero-crossing of the utility-line input voltage.

Fig. 20. Measured waveforms of rectified the utility-line input voltage $|\upsilon_{in}|$, the combined voltage waveform υ_O, and the rectified utility-line input current $|i_{in}|$.

Fig. 21. Experimental switch voltage υ_{DS} and current i_M waveforms of M_1 and M_2: (a) Near the peak of the utility-line input voltage. (b) Near the zero-crossing of the utility-line input voltage.

Fig. 22. Measured utility-line input voltage υ_{in}, utility-line input current i_{in}, input power p_{in} waveforms and load voltage V_{LED}, load current I_{LED}, output power P_{out} waveforms.

Fig. 23. Measured PF and THD_i under various utility-line input voltages and output powers of the proposed single-stage LED driver: (a) PF and THD_i as a function of the various utility-line input voltages at an output power of 150 W. (b) PF and THD_i as a function of various output powers at a line voltage of 220 V_{rms}.

Fig. 24. Measured efficiency under various utility-line input voltages and output powers of the proposed single-stage LED driver: (a) Efficiency as a function of various utility-line input voltages at an output power of 150 W. (b) Efficiency as a function of various output power at a line voltage of 220 V_{rms}.

Fig. 25. Simplified equivalent circuits of the PFC semi-stage with the junction capacitance effect of the ZCDS Class-E current-driven rectifier diode. (a) The ZCDS-CECS-RPFC with junction capacitance of the ZCDS Class-E current-driven rectifier diode. (b) Simplified equivalent circuit of (a). (c) Equivalent circuit when the parallel L_{sp}-R_{sp} circuit is transferred into series L_{ss}-R_{ss} circuit.

Table captions

TABLE I Comparison of Lighting Sources for Street-Lighting Systems

TABLE II Equivalent Circuit Operating Modes in One Switching Cycle of the ZCDS-CECS-RPFC

TABLE III Parameters of Proposed Single-Stage LED Driver based on the ZCDS-CECS-RPFC

TABLE IV Prototype Parameters of Proposed Single-Stage LED Driver based on the ZCDS-CECS-RPFC

TABLE V Measured Harmonic Content of the Utility-Line Input Current Compared with IEC 61000-3-2 Class-C

TABLE VI Key Performance Comparison Among RPFC Topologies

TABLE VII Comparative Study of Proposed LED Street-Light Driver with Presented Publications

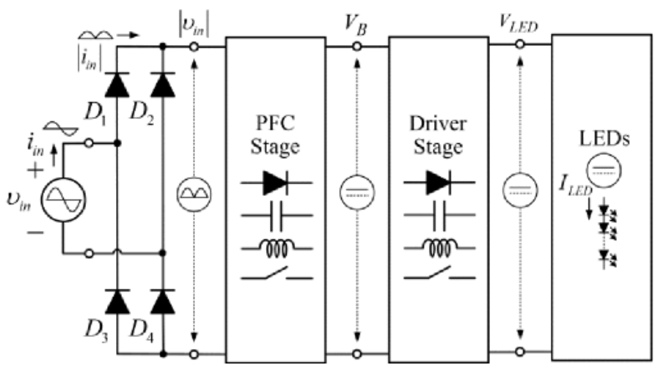

(a)

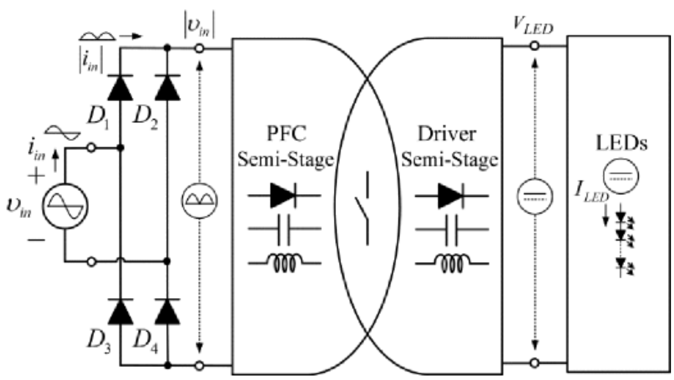

(b)

Fig. 1.

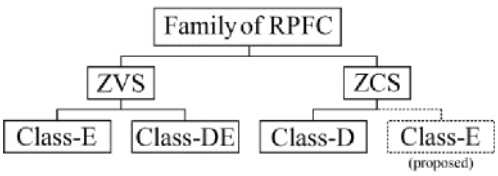

Fig. 2.

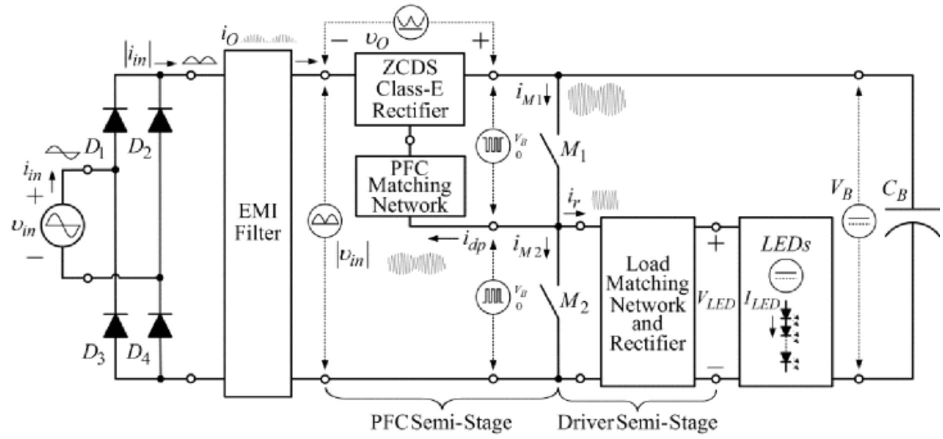

ZCDS
Class-E
Rectifier
PFC
Matching
Network
EMI
Filter
Load
Matching
Network
and
Rectifier
LEDs
PFC Semi-Stage
Driver Semi-Stage

Fig. 3.

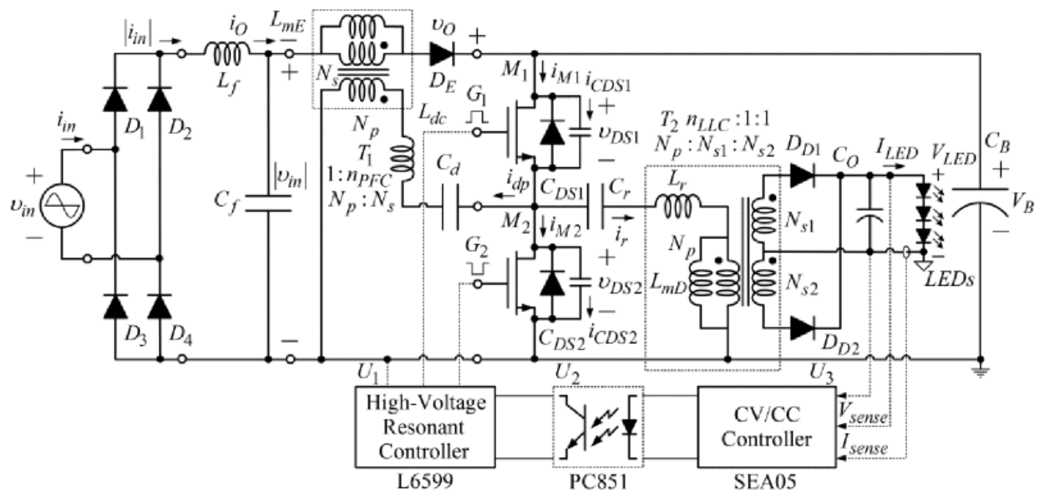

High-Voltage
Resonant
Controller
L6599
PC851
CV/CC
Controller
SEA05
LEDs

Fig. 4.

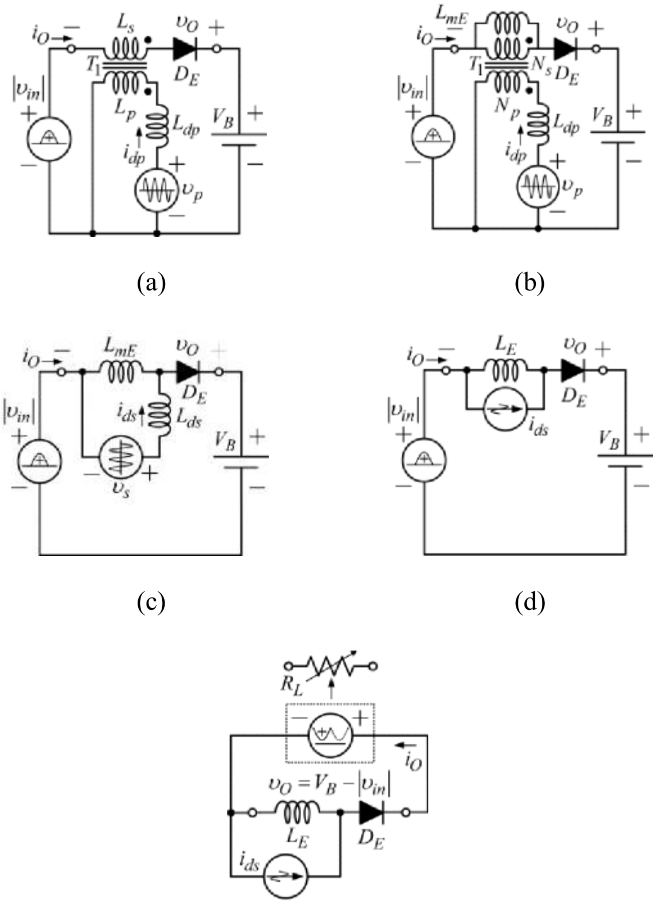

i_O
L_s
v_O
T_1
D_E
$|v_{in}|$
L_p
L_{dp}
V_B
i_{dp}
v_p
L_{mE}
N_s
N_p
i_{ds}
L_{ds}
v_s
L_E
R_L
$v_O = V_B - |v_{in}|$

(a) (b) (c) (d) (e)

Fig. 5.

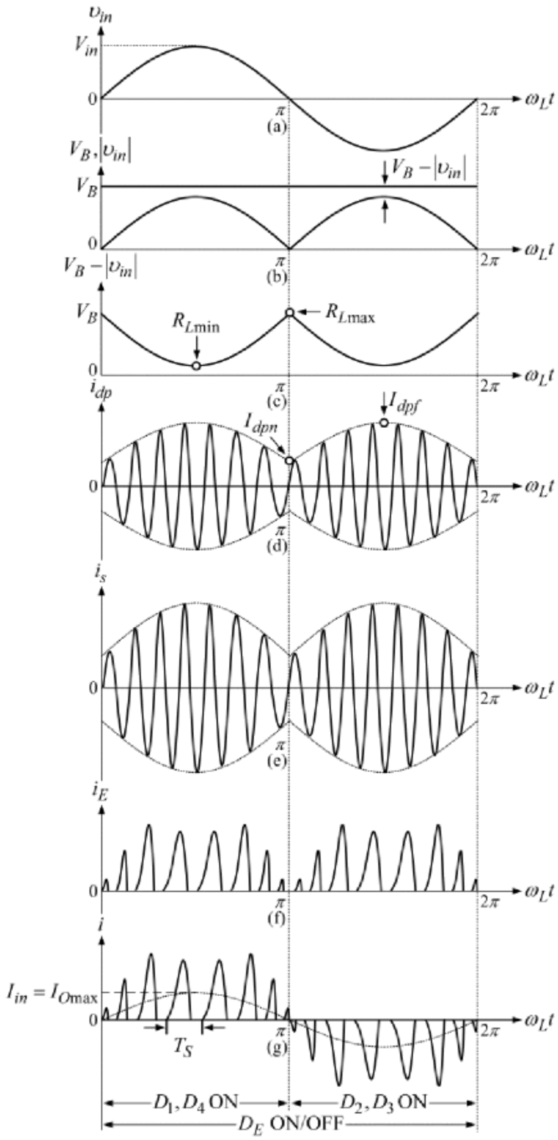

v_{in}
V_{in}
0
$\omega_L t$
π
(a)
2π
$V_B, |v_{in}|$
$V_B - |v_{in}|$
V_B
0
(b)
$V_B - |v_{in}|$
V_B
$R_{L\min}$
$R_{L\max}$
(c)
i_{dp}
I_{dpn}
I_{dpf}
(d)
i_s
(e)
i_E
(f)
i
$I_{in} = I_{O\max}$
T_S
(g)
D_1, D_4 ON
D_2, D_3 ON
D_E ON/OFF

Fig. 6.

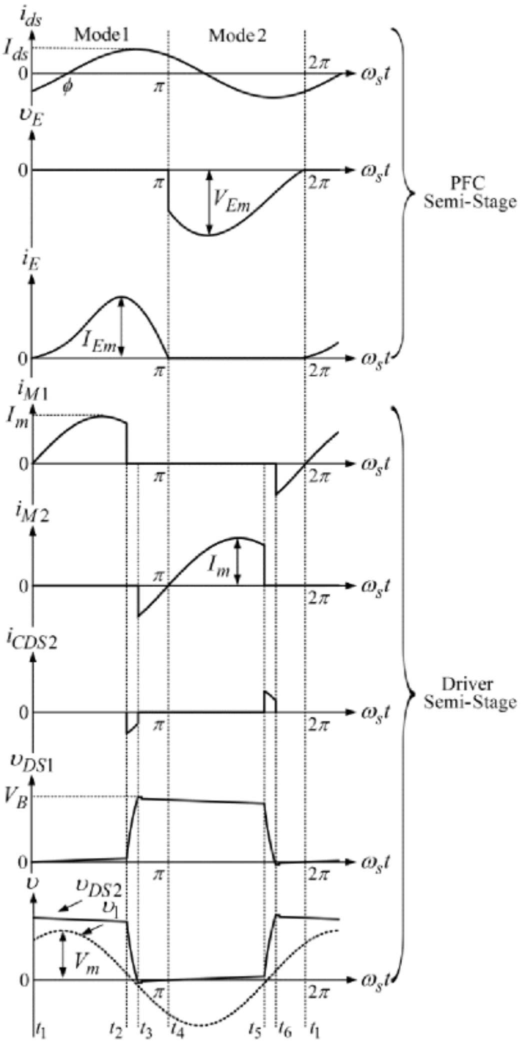

i_{ds}
Mode 1
Mode 2
I_{ds}
0
ϕ
π
2π
$\omega_s t$
υ_E
V_{Em}
PFC Semi-Stage
i_E
I_{Em}
i_{M1}
I_m
i_{M2}
i_{CDS2}
Driver Semi-Stage
υ_{DS1}
V_B
υ
υ_{DS2}
υ_1
V_m
t_1
t_2
t_3
t_4
t_5
t_6

Fig. 7.

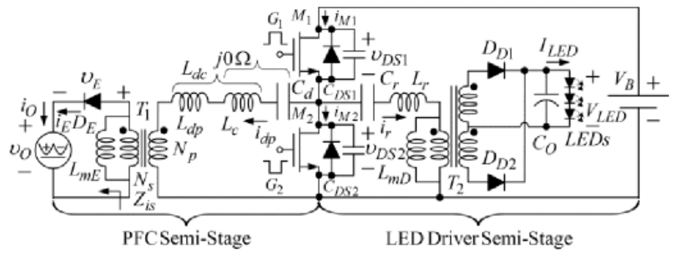

(a)

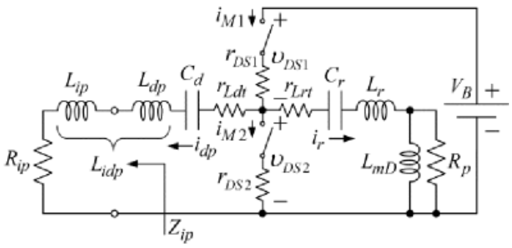

(b)

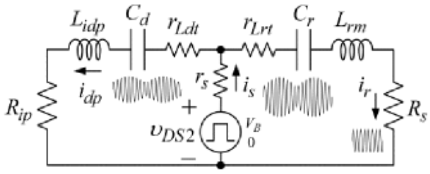

(c)

Fig. 8.

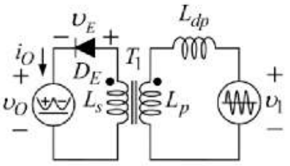

(a)

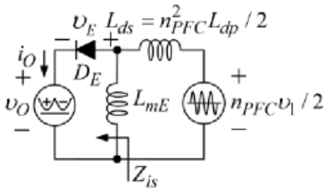

(b)

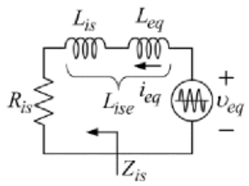

(c)

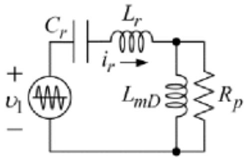

(d)

Fig. 9.

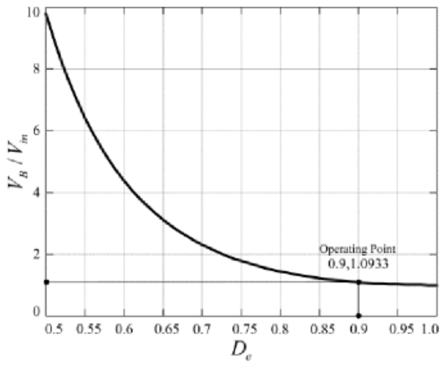
10
8
6
4
2
0
V_B / V_{in}
0.5 0.55 0.6 0.65 0.7 0.75 0.8 0.85 0.9 0.95 1.0
D_e
Operating Point
0.9,1.0933

Fig. 10.

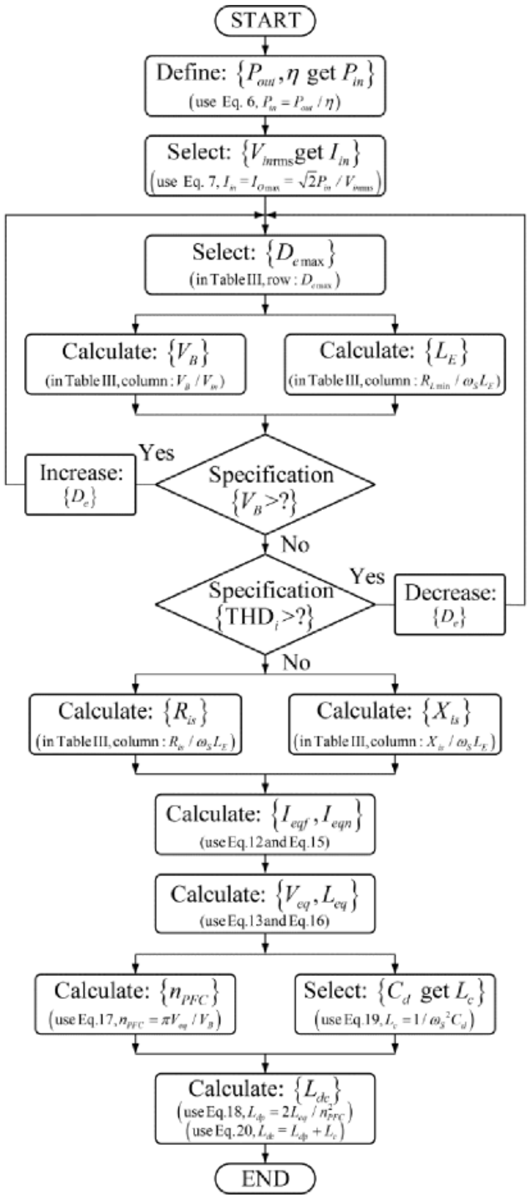
START
Define: $\{P_{out}, \eta$ get $P_{in}\}$
(use Eq. 6, $P_{in} = P_{out} / \eta$)
Select: $\{V_{inrms}$ get $I_{in}\}$
(use Eq. 7, $I_{in} = I_{O\max} = \sqrt{2} P_{in} / V_{inrms}$)
Select: $\{D_{e\max}\}$
(in Table III, row : $D_{e\max}$)
Calculate: $\{V_B\}$
(in Table III, column : V_B / V_{in})
Calculate: $\{L_E\}$
(in Table III, column : $R_{L\min} / \omega_S L_E$)
Yes
Increase: $\{D_e\}$
Specification $\{V_B > ?\}$
No
Specification $\{THD_i > ?\}$
Yes
Decrease: $\{D_e\}$
No
Calculate: $\{R_{is}\}$
(in Table III, column : $R_{is} / \omega_S L_E$)
Calculate: $\{X_{is}\}$
(in Table III, column : $X_{is} / \omega_S L_E$)
Calculate: $\{I_{eqf}, I_{eqn}\}$
(use Eq.12 and Eq.15)
Calculate: $\{V_{eq}, L_{eq}\}$
(use Eq.13 and Eq.16)
Calculate: $\{n_{PFC}\}$
(use Eq.17, $n_{PFC} = \pi V_{eq} / V_B$)
Select: $\{C_d$ get $L_c\}$
(use Eq.19, $L_c = 1 / \omega_S^2 C_d$)
Calculate: $\{L_{dc}\}$
(use Eq.18, $L_{dp} = 2 L_{eq} / n_{PFC}^2$)
(use Eq.20, $L_{dc} = L_{dp} + L_c$)
END

Fig. 11.

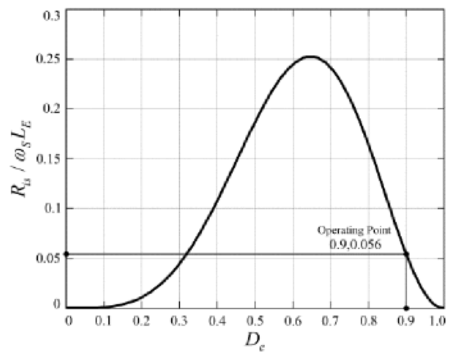

Fig. 12.

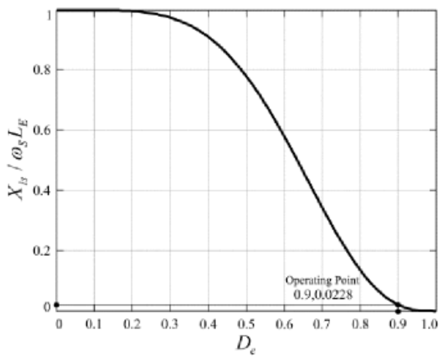

Fig. 13.

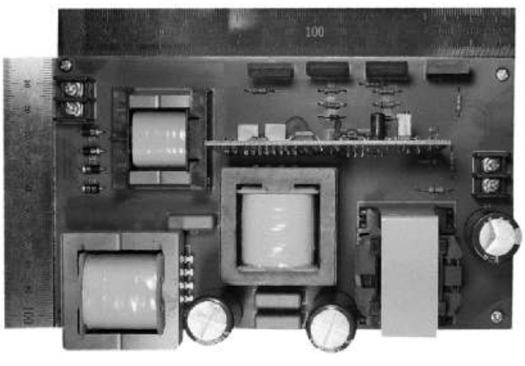

Fig. 14.

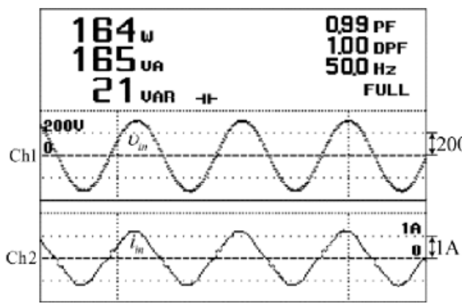

Fig. 15.

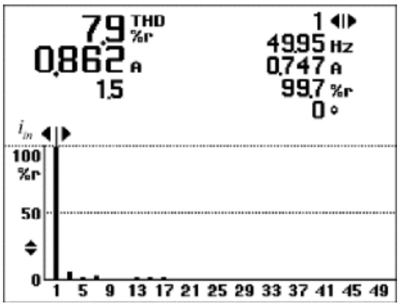

Fig. 16.

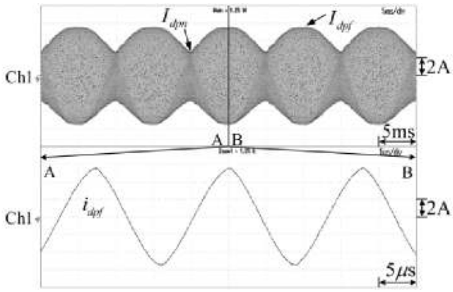

Fig. 17.

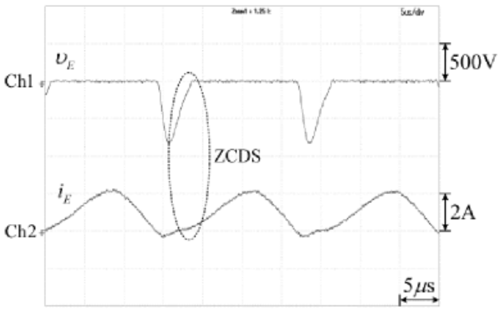

Fig. 18.

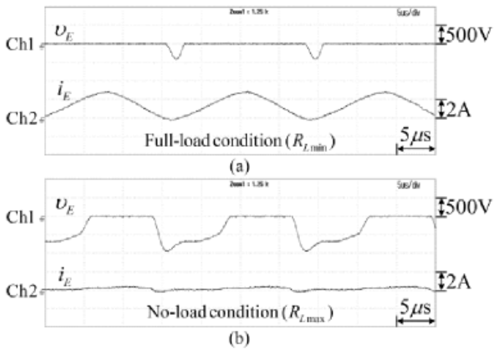

Fig. 19.

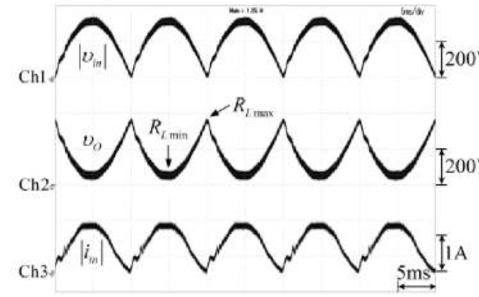

Fig. 20.

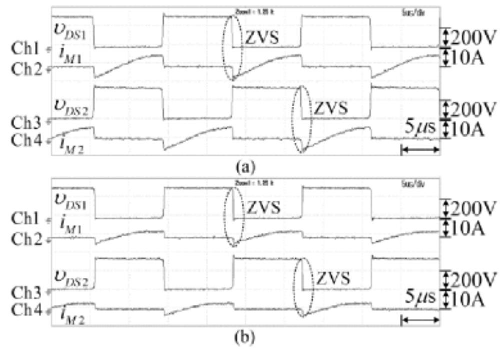

Fig. 21.

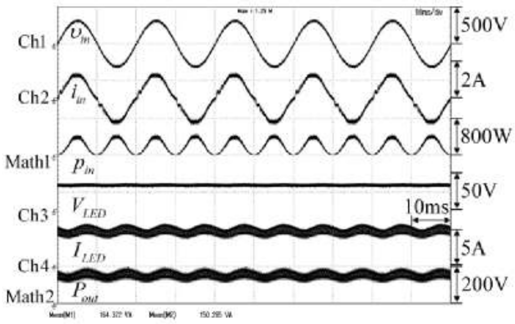

Fig. 22.

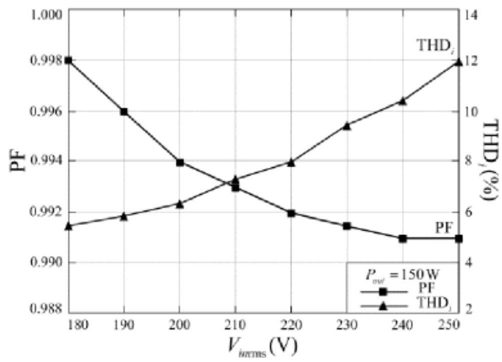

(a)

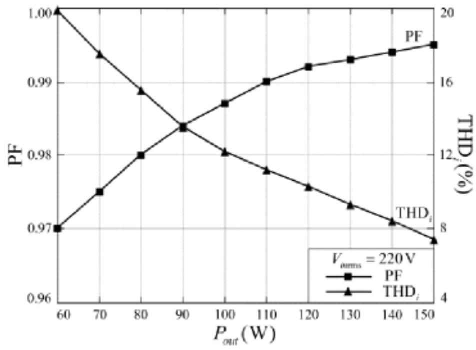

(b)

Fig. 23.

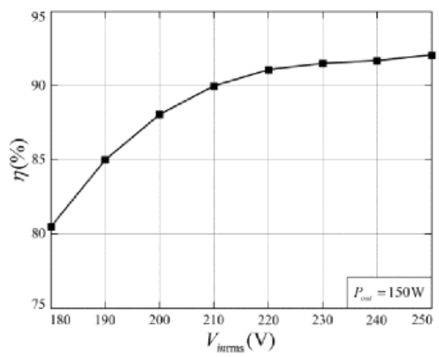

(a)

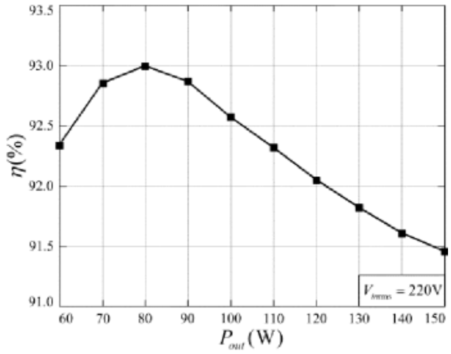

(b)

Fig. 24.

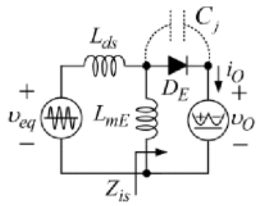

(a)

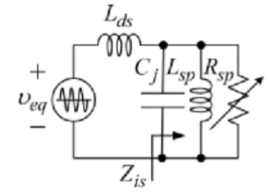

(b)

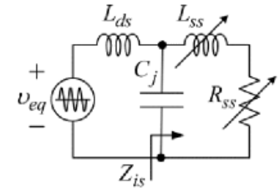

(c)

Fig. 25.

TABLE I

Items	High-Pressure Sodium Vapor Lamp	Metal Halide Lamp	HB-LED
Model	OSRAM NAV-T 150W	OSRAM HQI-E 150W	GENESIS LED Module 3×50W
Nominal Wattage	150 W	150 W	150 W
Efficacy	115 lm/W	83 lm/W	90 lm/W
Luminous Flux	17,500 lm	12,500 lm	14,000 lm
Color Rendering Index	25	88	70
Color Temperature	2,000 K	4,200 K	6,000 K
Light Appearance	Warm White	Cool White	Daylight
Lifespan	> 2,400 hours	> 6,000 hours	> 50,000 hours

TABLE II

Mode	Positive Input Utility-Line Half-Cycle	Negative Input Utility-Line Half-Cycle
	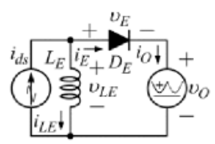	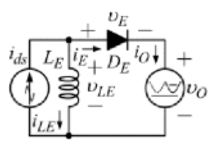
Mode 1	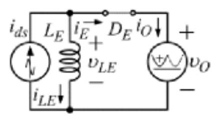	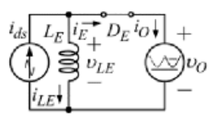
Mode 2	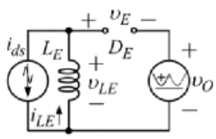	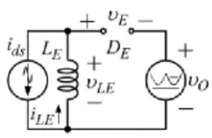

TABLE III

D_{emax}	V_B/V_{in}	$R_{Lmin}/\omega_S L_E$	$R_{is}/\omega_S L_E$	$X_{is}/\omega_S L_E$	R_{is}/R_{Lmin}	L_{is}/L_E
0	∞	∞	0	1	0	1
0.1	8.01×10^3	2865.3	0.0007	0.999	0.0002×10^{-3}	0.999
0.2	481.620	171.88	0.0097	0.996	0.0566×10^{-3}	0.996
0.3	89.390	31.611	0.4190	0.976	1.3260×10^{-3}	0.976
0.4	26.091	8.9734	0.1045	0.915	11.650×10^{-3}	0.915
0.5	9.7845	3.1416	0.1836	0.788	58.440×10^{-3}	0.788
0.6	4.3786	1.2083	0.2433	0.590	201.40×10^{-3}	0.590
0.7	2.3017	0.4655	0.2427	0.354	521.40×10^{-3}	0.354
0.8	1.4418	0.1580	0.1669	0.142	1056.5×10^{-3}	0.142
0.9	1.0933	0.0334	0.0560	0.022	1678.8×10^{-3}	0.022
1	1	0	0	0	2000.0×10^{-3}	0

TABLE IV

Symbol	Part Number or Value	Type
	Bridge-Rectifier and EMI Filter	
D_1-D_4	1N5395	Standard-Recovery Diode
L_f	5 mH	N87 EE32/16/9
C_f	680 nF/400 V	Polypropylene
	PFC Stage	
D_E	GB10MPS17	Silicon Carbide Schottky Diode
T_1	L_p = 92 μH, L_s = 2.5 mH	N87 EE42/21/15
L_{dc}	340 μH	N87 EE42/21/15
C_d	33 nF/1,000 V	Polypropylene
	Driver Stage	
M_1-M_2	IRFP460	N-Channel MOSFET
D_{D1}-D_{D2}	STPS40H100CW	Silicon Schottky Diode
T_2	L_r = 270 μH, L_{mD} = 1.4 mH	N87 EE42/21/20
C_r	30 nF/1,000 V	Polypropylene
C_O	100 μF/50 V	Electrolytic
C_B	240 μF/400 V	2 Parallel Connected of 120 μF Electrolytic Capacitors
LEDs	50W/32V	3 Parallel Connected of LED Street-Light Modules
	Control Stage	
U_1	L6599	High-Voltage Resonant Controller
U_2	PC851	Photocoupler
U_3	SAE05	CV/CC Controller

TABLE V

Harmonic Number (n)	IEC 61000-3-2 Class-C (%)	Experimental Result at P_{out} = 60 W (%)	Experimental Result at P_{out} = 150 W (%)
2	2	0.1	0.1
3	29.1	16.6	9.1
5	10	6.9	0.7
7	7	6.1	2.7
9	5	3.1	0.1
11	3	0.3	0.1
13	3	1.4	0.5
$15 \le n \le 39$	3	< 2.9	< 0.5

TABLE VI

Circuit Topology	ZVDS-CECS [34]	ZVDS-CDECS [35]	ZCS-CDCS [38]	ZCDS-CECS (proposed)
AC Line Voltage (V_{rms})	120	220	220	220
Max. Output Power (W)	32	36	34	150
Voltage Ratio V_B/V_{in}	1.27	1.051	1.1	1.093
Power Factor	0.99	0.99	0.98	0.99
Line Current THD (%)	12.6	1.3	20	7.9
Efficiency (%)	88.3	90	93.5	91.4
Normalized Driving Current I_{eqn}/I_{in} at Zero-Crossing of υ_{in}	3.87	6.36	0	0.39
Normalized Diode Current Stress I_D/I_{in}	3.61	6.36	3.14	2.08
Normalized Diode Voltage Stress V_D/V_B	2	1	1	2
Diode	1	2	2	1
Inductor	1	1	1	1
Capacitor	2	3	1	1
Transformer	1	0	0	1
Component Count	5	6	4	4

TABLE VII

Item	Two-Stage [3]	Two-Stage [8]	Two-Stage [9]	Single-Stage (proposed)
AC Line Voltage (V_{rms})	120	90~264	220	180~250
Output Voltage (V)	95	43	27	32
DC-Bus Voltage (V)	400	N/A	400	340
Max. Output Power (W)	40	150	100	150
PF	N/A	0.98	N/A	0.99
THD_i (%)	N/A	16	N/A	7.9
η (%)	91.5	89.9	94.5	91.4
Power Switch	3	3	3	2
Diode	7	7	7	7
Capacitor	5	4	5	5
Inductor	3	3	4	2
Transformer	1 (with L_m and L_r)	1 (with L_m)	1 (with L_m)	2 (with L_{mE}, L_{mD} and L_r)
Controller	2	2	2	1
Component Count	21	20	22	19